NUMERICAL INVESTIGATION OF THE THREE-DIMENSIONAL LAMINAR BOUNDARY LAYER WITH COUPLED HEAT TRANSFER

V. I. Zinchenko and O. P. Fedorova

UDC 533.526 + 536.24

The authors examine heating of a spherically blunted cone washed by a flow in chemical equilibrium or a supersonic air flow, allowing for interaction of the gas processes with the surface, i.e., the coupled form of the problem. It is difficult to use a decoupled formulation of the problem, taking the heat-transfer coefficient from the gas phase to calculate the heat conduction in the body, since there are no reliable data for α for three-dimensional flow over nonisothermal surfaces.

1. Following [1, 2] we shall seek the characteristics of the coupled heat transfer by solving the system of equations of the three-dimensional boundary layer and the unsteady heat-conduction equation in the body shell, with the appropriate boundary and initial conditions. For the perfect gas model the system of equations of the laminar three-dimensional boundary layer has been given in [3]. For associated air, under the hypothesis of a binary mixture it is easy to show that the element concentrations for a nonablating wall are constant in the boundary layer and equal to their values in the incident stream. The calculation of the equilibrium state can proceed autonomously and the transfer coefficients and the molecular weight of the mixture can be approximated as functions of p and T or of p and h [4], and can then be used in integration of the system of boundary layer equations.

In the general case of multicomponent diffusion the elementary composition varies in the boundary layer [5], and this must be accounted for in solving specific problems. For a dissociated air mixture, when the flow quantities have been obtained, the assumption that the elementary composition does not change in the boundary layer can be used with quite good accuracy.

In accordance with [6], the boundary layer on the spherical part of the body in the coordinate system fixed at the stagnation point was calculated for the symmetric case, and then we converted to a semigeodesic coordinate system fixed with the body symmetry axis. In Dorodnitsyn–Lees variables, after introducing the stream functions f and φ, the system of equations of the three-dimensional boundary layer has the form

$$\frac{\partial}{\partial\zeta}\left(l\frac{\partial\bar{u}}{\partial\zeta}\right)+(\alpha_4 f+\alpha_3\varphi)\frac{\partial\bar{u}}{\partial\zeta}=\alpha_1\left(\bar{u}\frac{\partial\bar{u}}{\partial\xi}-\frac{\partial f}{\partial\xi}\frac{\partial\bar{u}}{\partial\zeta}\right)+\alpha_2\left(\bar{\omega}\frac{\partial\bar{u}}{\partial\eta}-\frac{\partial\varphi}{\partial\eta}\frac{\partial\bar{u}}{\partial\zeta}\right)+\beta_1\left(\bar{u}^2-\frac{\rho_e}{\rho}\right)+\beta_2\left(\bar{\omega}^2-\frac{\rho_e}{\rho}\right)+\beta_3\left(\overline{u\omega}-\frac{\rho_e}{\rho}\right) \quad (1.1)$$

$$\frac{\partial}{\partial\zeta}\left(l\frac{\partial\bar{\omega}}{\partial\zeta}\right)+(\alpha_4 f+\alpha_3\varphi)\frac{\partial\bar{\omega}}{\partial\zeta}=\alpha_1\left(\bar{u}\frac{\partial\bar{\omega}}{\partial\xi}-\frac{\partial f}{\partial\xi}\frac{\partial\bar{\omega}}{\partial\zeta}\right)+\alpha_2\left(\bar{\omega}\frac{\partial\bar{\omega}}{\partial\eta}-\frac{\partial\varphi}{\partial\eta}\frac{\partial\bar{\omega}}{\partial\zeta}\right)+\beta_4\left(\bar{\omega}^2-\frac{\rho_e}{\rho}\right)+\beta_5\left(\overline{u\omega}-\frac{\rho_e}{\rho}\right); \quad (1.2)$$

$$\frac{\partial}{\partial\zeta}\left\{\frac{l}{\mathrm{Pr}}\frac{\partial g}{\partial\zeta}+\gamma_1 l\left(1-\frac{1}{\mathrm{Pr}}\right)\frac{\partial}{\partial\zeta}\left[\bar{u}^2+\left(\frac{\omega_e}{u_e}\bar{\omega}\right)^2\right]\right\}+(\alpha_4 f+\alpha_3\varphi)\frac{\partial g}{\partial\zeta}=\alpha_1\left(\bar{u}\frac{\partial g}{\partial\xi}-\frac{\partial f}{\partial\xi}\frac{\partial g}{\partial\zeta}\right)+\alpha_2\left(\bar{\omega}\frac{\partial g}{\partial\eta}-\frac{\partial\varphi}{\partial\eta}\frac{\partial g}{\partial\zeta}\right). \quad (1.3)$$

Assuming that the process is one-dimensional we write the unsteady heat-conduction equation in the body material in the orthogonal semigeodesic coordinate system as

$$\pi_\rho\frac{\partial\theta}{\partial\tau}=\frac{1}{H_1 r_1}\frac{\partial}{\partial n_1}\left[H_1 r_1\pi_\lambda\frac{\partial\theta}{\partial n_1}\right]. \quad (1.4)$$

The boundary and initial conditions are as follows:

$$\bar{u}(\xi,\eta,\infty)=1,\ \bar{\omega}(\xi,\eta,\infty)=1,\ g(\xi,\eta,\infty)=1, \quad (1.5)$$
$$\bar{u}(\xi,\eta,0)=0,\ \bar{\omega}(\xi,\eta,0)=0,\ f(\xi,h,0)=\varphi(\xi,\eta,0)=0;$$

Tomsk. Translated from Zhurnal Prikladnoi Mekhaniki i Tekhnicheskoi Fiziki, No. 2, pp. 34-42, March-April, 1988. Original article submitted November 19, 1986.

0021-8944/88/2902-0189$12.50

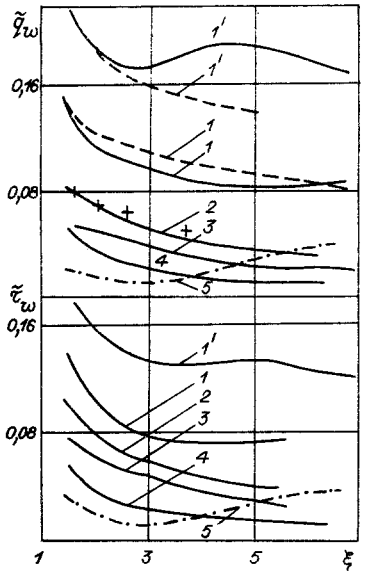

Fig. 1

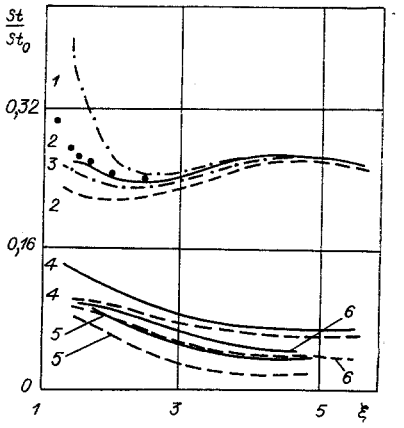

Fig. 2

$$\tilde{q}_w(\xi, \eta, 0)\frac{H_{e0}\sqrt{V_m\rho_{e0}\mu_{e0}R_N}}{\lambda_{1*}T_*} - \pi_\sigma\theta_w^4 = -\pi_\lambda(\theta_w)\frac{\partial\theta}{\partial n_1}(\tau, 0); \tag{1.6}$$

$$\frac{\partial\theta}{\partial n_1}\left(\tau, \frac{L}{R_N}\right) = 0 \quad \text{or} \quad \theta\left(\tau, \frac{L}{R_N}\right) = \theta_н,\ \theta(0, n_1) = \theta_н. \tag{1.7}$$

Here ξ is the dimensionless path length, calculated from the symmetry axis; η, an angle calculated from the windward side in the body symmetry plane, in deg; and $\zeta = \frac{u_e r_w}{N}\int_0^n \rho dn$, $n_1 = -\frac{n}{R_N}$ are directed along the normal to the exterior profile on the different sides; $g = H/H_{e0}, \bar{u} = \partial f/\partial\zeta = u/u_e, \bar{\omega} = \partial\varphi/\partial\zeta = \omega/\omega_e$ are the dimensionless enthalpy and velocity components in the longitudinal and circumferential directions;

$$\alpha_1 = \frac{2\int_0^\xi \rho_e\mu_e u_e r_w^2 d\xi}{\rho_e\mu_e u_e r_w^2},\quad \alpha_2 = \frac{\omega_e}{u_e\bar{r}_w}\alpha_1,$$

$$\alpha_3 = \frac{\alpha_1}{\bar{r}_w}\frac{\partial}{\partial\eta}\left(\frac{\omega_e}{u_e}\right) + \frac{\omega_e}{\rho_e\mu_e u_e^2\bar{r}_w}\frac{\partial}{\partial\eta}\left(\int_0^\xi \rho_e\mu_e u_e\bar{r}_w^2 d\xi\right),$$

$$\alpha_4 = 1,\ \beta_1 = \frac{\alpha_1}{u_e}\frac{\partial u_e}{\partial\xi},\ \beta_2 = -\alpha_1\left(\frac{\omega_e}{u_e}\right)^2\frac{1}{\bar{r}_w}\frac{d\bar{r}_w}{d\xi},\ \beta_3 = \alpha_2\frac{1}{u_e}\frac{\partial u_e}{\partial\eta},\ \beta_4 = \frac{\alpha_2}{\omega_e}\frac{\partial\omega_e}{\partial\eta},$$

$$\beta_5 = \alpha_1\left(\frac{1}{\bar{r}_w}\frac{\partial\bar{r}_w}{\partial\xi} + \frac{1}{\omega_e}\frac{\partial\omega_e}{\partial\xi}\right),\ l = \frac{\rho\mu}{\rho_e\mu_e},\ \bar{r}_w = \frac{r_w}{R_N},\ \gamma_1 = \frac{u_e^2}{2H_{e0}},\ \pi_\rho = \frac{\rho_1 c_1}{\rho_{1*}c_{1*}},$$

$$\pi_\lambda = \frac{\lambda_1}{\lambda_{1*}},\ \pi_\sigma = \frac{\varepsilon\sigma T_*^3}{\lambda_{1*}}$$

are dimensionless coefficients and parameters; $\tilde{q}_w = \frac{\mu_w}{\mathrm{Pr}_w}\frac{\partial H}{\partial n}\Big|_w\left(\frac{R_N}{\sqrt{V_m\rho_{e0}\mu_{e0}}}\right)^{1/2}\frac{1}{H_{e0}}$, $\theta = \frac{T}{T_*}$, $\tau = \frac{t}{t_*}$ are the dimensionless heat flux, temperature and time; $t_* = \frac{R_N^2\rho_{1*}c_{1*}}{\lambda_{1*}}$, $V_m = \sqrt{2H_{e0}}$, R_N, L are the characteristic time and velocity, radius of blunting, and shell thickness; $H_1 = 1 - kn$, $r_1 = r_w - n_1\cos\vartheta$ are Lamé coefficients (k is the curvature of the generator, θ the slope angle of the body generator to the symmetry axis); the subscripts e, e0 and w denote values at the outer

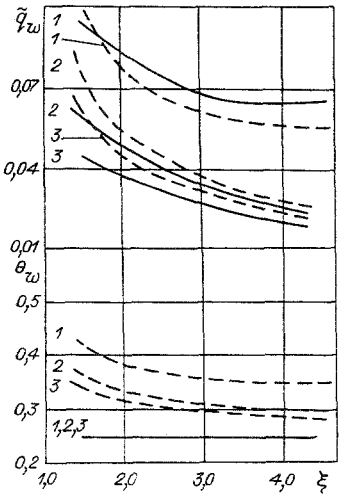

Fig. 3

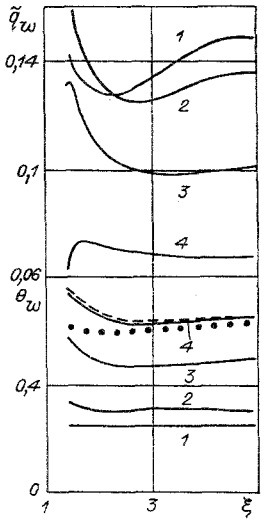

Fig. 4

edge of the boundary layer, at the outer edge at the stagnation point, and on the body surface, and the subscripts 1, * are the characteristics of the solid phase and characteristic values.

For the perfect gas model as the temperature T_* it is convenient to use T_{e0}, and then $\frac{H_{e0}\sqrt{V_m\rho_{e0}\mu_{e0}R_N}}{\lambda_{1*}T_*} = \sqrt{\mathrm{Re}}\,\mathrm{Pr}\frac{\lambda_{e0}}{\lambda_{1*}}$, $\mathrm{Re} = \frac{V_m\rho_{e0}R_N}{\mu_{e0}}$. The parameter $S = \sqrt{\mathrm{Re}}\mathrm{Pr}\,\lambda_{e0}/\lambda_{1*}$ is used for coupled heat-transfer problems.

For the equilibrium air model in writing the system of equations and the boundary condition (1.6) we assume a Lewis number of 1. The equation of state and $\rho\mu$ were taken from [4]. At the outer edge of the boundary layer we assumed ths conditions from the inviscid flow calculations of [7] and approximated with the help of two-dimensional matching splines [8].

The difference schemes for the computed regions in the gas phase and in the body were obtained with the help of the iteration-interpolation method (IIM) [9], with an approximation error of $O(\Delta\zeta)^2 + O(\Delta\xi) + O(\Delta\eta)$, $O(\Delta n_1)^2 + O(\Delta\tau)$.

To solve coupled problems requires multiple calculation of the system of equations of the three-dimensional boundary layer, and it is therefore important to optimize to chosen schemes and to accelerate the convergence in practice we used the technique of [10] to analyze a number of difference schemes and IIM schemes comparatively, and we showed that the IMM schemes have second-order convergence rate. The method of calculation is associated with the quasisteady nature of the processes in the gas phase, and consists of sequential solution of the system of equations in the gas phase and the heat-conduction equation in the body. In integrating Eqs. (1.1)-(1.3) with respect to η as initial conditions we used the solution of the asymptotic system of equations written in the vicinity of the flow symmetry plane.

In the numerical calculations made we investigated assigning the angle of attack χ and the coupling parameter S, and we analyzed the influence of the nonisothermal nature of the surface temperature on the heat flux and the heat-transfer coefficient.

2. We now consider the results of solving the boundary problem of Eqs. (1.1)-(1.3), (1.5), and (1.6) for the perfect gas model and the Sutherland law for μ in the case of a given surface temperature. Figure 1 shows the distributions of dimensionless heat flux $\tilde{q}_w$ and friction stress $\tilde{\tau}_w = \mu_w[(\partial u/\partial n|_w)^2 + (\partial\omega/\partial n|_w)^2]\sqrt{\mathrm{Re}}/(\rho_{e0}V_m^2)$ along the generators of the conical part at different meridional sections η. Here $\chi = 10°$, $\gamma = 1$, 4, $g_w = \theta_w = 0.05$ and the body geometry (the semivertex angle $\vartheta = 10°$) and M_∞ are taken from [3]. Curves 1-4 correspond to $\eta = 0$, $\pi/2$, 2.27, π, respectively, and curves 1′ were obtained in the vicinity of the plane of symmetry on the windward side $\eta = 0$ for the same governing parameters of the problem, apart from $\chi = 20°$. As can be seen from Fig. 1, the maximum values of heat flux and friction stress are reached on the flow symmetry line $\eta = 0$, where the pressure is a maximum. Because of the secondary stagnation of the flow on the windward side of the conical surface the

pressure along the generator increases, leading to an increase of $\tilde{q}_w$ and $\tilde{\tau}_w$ and depend substantially on the angle of attack.

Along the meridional section $\eta = \pi/2$ the heat flux is close to the calculated value $\tilde{q}_w(\xi)$ (shown by crosses) obtained for axisymmetric flow over the same cone. Hence it follows that on a given meridian for the value of χ used the divergence of the streamlines at the outer edge of the boundary layer and near the body surface does not play a large part in determining the local heat flux, as was discovered experimentally in [11].

In the vicinity of the line of flow divergence it is interesting to compare $\tilde{q}_w$ with the results of calculations of axisymmetric flow for the same local angles of attack. In this case $\chi = 0$, $\vartheta = 20°$, and $\vartheta = 30°$ for the broken curves 1 and 1', respectively. The pressure at the outer edge is different because of overflow of the gas in the circumferential direction for $\chi \neq 0$ with increase of angle of attack there is an increased pressure gradient in the circumferential direction, leading to an increased intensity of the secondary flows and an increased error in the axisymmetric calculation for the equivalent cone.

Calculations performed in the vicinity of the symmetry plane on the leeward side have shown that, beginning with certain values of ξ, corresponding to the appearance of the maximum of vector $p_e(\eta)$ became negative, which is typical of a change of direction of the flow within the boundary layer with respect to the symmetry plane. The change of flow direction leads to flow rearrangement and to formation of a region of flow spreading, which may be accompanied, for increased angle of attack, by an increase of heat flux and friction stress. The lines 5 on Fig. 1 show the distributions of $\tilde{q}_w(\xi), \tilde{\tau}_w(\xi)$ for $\eta = \pi$ for the parameters of [11] ($M_\infty = 5$, $\chi = 20$, $9°$, $\vartheta = 9°$), which confirms what has been said above. This kind of behavior of $\tilde{q}_w(\xi)$ for $\eta = \pi$ was noted in a number of experimental studies, and a calculation performed according to the data of [12] has shown agreement between the theoretical and experimental results. We shall consider the influence of assigning an isothermal surface temperature on the flow characteristics in the boundary layer. Figure 2 shows the ratio $\frac{\mathrm{St}}{\mathrm{St}_0} = \frac{q_w(\xi, \eta)[1-\theta_{w0}]}{q_{w0}[1-\theta_w(\xi, \eta)]}$ along the coordinate ξ for various values of η (curves 2, 4 for $\eta = 0$; 5 and 6 for $\eta = \pi/2$). Here q_{w0}, θ_{w0} correspond to values at the stagnation point, curves 2 and 5 were obtained for $\chi = 20°$; and curves 4 and 6 for $\chi = 5°$. The solid lines correspond to $\theta_w = 0.05$, and the broken lines to $\theta_w = 0.5$. The other governing parameters coincide with the data of Fig, 1. It can be seen that with increase of θ_w by an order the value of $\mathrm{St}/\mathrm{St}_0$ decreases in all the meridional sections and there is a tendency towards an increased influence of the change of the temperature factor on the relative heat flux for an increase of χ. The data of [13] are shown by the points at $\eta = 0$, $\chi = 20°$, $\theta_w = 0.248$, according to which in the vicinity of the line of spreading

$$\frac{\mathrm{St}}{\mathrm{St}_0} = \frac{0.8\dfrac{p_e}{p_{e0}}\dfrac{u_e}{V_m}\left[\theta_e + \sqrt{\mathrm{Pr}}\left(\dfrac{u_e}{V_m}\right)^2 - \theta_w\right]}{k^{0.5}\left(\dfrac{r_w}{R_N}\right)^{0.3}[1-\theta_{w0}]}. \tag{2.1}$$

For the model of an ideal gas:

$$k = \frac{\gamma-1}{\gamma+1}, \quad \theta_e = \frac{T_e}{T_{e0}} = \left(\frac{p_e}{p_{e0}}\right)^{\frac{\gamma-1}{\gamma}}, \quad \left(\frac{u_e}{V_m}\right)^2 = 1 - \left(\frac{p_e}{p_{e0}}\right)^{\frac{\gamma-1}{\gamma}}$$

As follows from Figs. 1 and 2 the heat flux distribution on the wetted surface is complex, and is determined by the formation $T_w(\xi, \eta)$ and the temperature fields in the body material in solving the heating problem. The results of solving the coupled problem are shown in Fig. 3 for $\theta_H = 0.248$, $T_{e0} = 1210$ K, $\sqrt{\mathrm{Re}\,\mathrm{Pr}}\frac{\lambda_{e0}}{\lambda_{1*}} = 3.187$. (the other parameters are the same as for Fig. 1). The thermophysical characteristics of the material were assumed constant, $L/R_N = 0.1$, $\partial\theta/\partial n_1(\tau, L/R_N) = 0$. The dependences $\tilde{q}_w(\xi, \eta)$ and $\theta_w(\xi, \eta)$ were found at different times τ, the solid curves correspond to $\tau = 0$, and the broken curves correspond to $\tau = 0.046$, curves 1-3 being for $\eta = 0$, $\pi/2$, 2.27.

For the times indicated it is interesting to note the increase of heat flux, more noticeable in the region with coupling of the spherical and conical part of the body. The increase

of $\tilde{q}_w(\xi, \eta)$ stems from the fact that at times close to the initial time θ_w changes from θ_i = const to a nonisothermal distribution $\theta_w(\xi, \eta)$, which in turn leads to an increase of the heat-transfer coefficient to the body and an increased heat flux. For a further increase of T_w because of the decrease of the temperature drop $T_{e0} - T_w(\xi, \eta)$, the value of $\tilde{q}_w(\xi, \eta)$ begins to decrease.

Figure 4 shows the results of solving the coupled problem in the most thermally stressed region for $\eta = 0$, which illustrates the above behavior of $\tilde{q}_w$. The calculation parameters were chosen to be the same as for Fig. 3, apart form $\chi = 20°$, and curves 1-4 correspond to $\tau = 0$, 0.01, 0.051, 0.108.

The influence of the nonisothermal nature of the surface temperature on the heat-transfer coefficient is shown in Fig. 2, which shows a representation of the numerical solution given in Fig. 4 in the form of the ratio St/St_0 for $\tau = 0.01$ and 0 (curves 1 and 3). It can be seen that for the constant and variables surface temperatures the values of St/St_0 differ substantially, while for the isothermal surface and a parametric set of data the difference in St/St_0 does not exceed 15%.

The nonmonotonic behavior of $\tilde{q}_w(\tau)$ stemming from the nonisothermal surface temperature distribution can be seen from the analytical solution in the vicinity of the plane of symmetry, obtained with the help of the method of successive approximations [14] for variable temperature $\theta_w(\xi)$:

$$\frac{q_w(\xi)}{q_w(\xi_*)} = \sqrt{\frac{\rho_e\mu_e u_e \delta_g(\xi_*)}{2\frac{du_e}{d\xi}\Big|_{\xi=\xi_*}\rho_{e0}\mu_{e0}\alpha\delta_g(\xi)}}\frac{B(\xi_*)}{B(\xi)}\left\{(1-\psi)+2\mathrm{Pr}\,\delta_g(\xi)\alpha B(\xi)\beta\left(1-\frac{\Phi_1}{2B(\xi)}\right)\right\}\frac{1-g_w(\xi)}{1-g_w(\xi_*)},$$

$$\Phi_1 = 0{,}068 + 0{,}091A, \quad B(\xi) = 0.068 + 0.057A,$$
$$\beta = \frac{\partial \ln(1-g_w)}{\partial\xi}, \quad \psi = \frac{1-\mathrm{Pr}}{1-g_w}\left(\frac{u_e}{V_m}\right)^2, \quad A = \left(\frac{g_w}{1-\left(\frac{u_e}{V_m}\right)^2}\right)^{0.5}, \quad m = \rho_e\mu_e u_e \bar{r}_w^2, \tag{2.2}$$

$$E = \exp\left(2\int_{\xi_*}^{\xi}\frac{\omega_e}{u_e}\frac{1}{r_w}d\xi\right), \quad \alpha = \frac{\int_{\xi_*}^{\xi}\rho_e\mu_e u_e r_w^2 d\xi}{\rho_e\mu_e u_e r_w^2}; \tag{2.3}$$

$$\delta_g(\xi) = \left[\int_{\xi_*}^{\xi}\frac{(1-\psi)m}{\mathrm{Pr}\,B(\xi)}\exp\left(\int_{\xi_*}^{\xi}\beta\frac{\Phi_1}{B(\xi)}d\xi\right)Ed\xi\right]\left[\alpha mE\exp\left(\int_{\xi_*}^{\xi}\beta\frac{\Phi_1}{B(\xi)}d\xi\right)\right]^{-1}.$$

Here ξ_* is the coordinate of the stagnation point, and for $\delta_g(\xi_*)$, expanding the functions in the vicinity of the stagnation point, we can write

$$\delta_g(\xi_*) = \frac{1}{\mathrm{Pr}\,B(\xi_*)\left(1+\frac{R_1(\xi_*)}{R_2(\xi_*)}\right)}, \quad B(\xi_*) = 0.068 + 0.057g_{w0}^{0.5}$$

($R_1(\xi_*)$, $R_2(\xi_*)$ are the principal radii of curvature at the stagnation point). In the case of spherical blunting for $\xi_* \le \xi \le \xi_1$, where ξ_1 corresponds to the coordinate of transition to the conical part of the body,

$$\omega_e = u_e\frac{\sin\xi_*}{\sin(\xi-\xi_*)},$$

and for this region

$$\delta_g(\xi) = \left[\int_{\xi_*}^{\xi}\frac{(1-\psi)m}{\mathrm{Pr}\,B(\xi)}\exp\left(\int_{\xi_*}^{\xi}\beta\frac{\Phi_1}{B(\xi)}d\xi\right)\frac{(\mathrm{tg}\,\xi-\mathrm{tg}\,\xi_*)^2}{\mathrm{tg}^2\,\xi}d\xi\right]\left[\alpha m\exp\left(\int_{\xi_*}^{\xi}\frac{\Phi_1}{B(\xi)}d\xi\right)\frac{(\mathrm{tg}\,\xi-\mathrm{tg}\,\xi_*)^2}{\mathrm{tg}^2\,\xi}\right]^{-1}. \tag{2.4}$$

As follows from analysis of Eq. (2.2), and also from the results of the numerical solutions, the second term in Eq. (2.2), associated with $\partial g_w/\partial\xi$, can make an appreciable contribution to the value of the heat-transfer coefficient for a nonisothermal surface. In the region of positive values of $\partial g_w/\partial\xi$ the ratio St/St_0 decreases, and for negative values it increases compared with the isothermal case. This can lead to a decrease of θ_w in regions where $\partial\theta_w/\partial\xi < 0$, in calculating the temperature field in the body using the heat-transfer coefficient from the gas phase, as found for the isothermal surface.

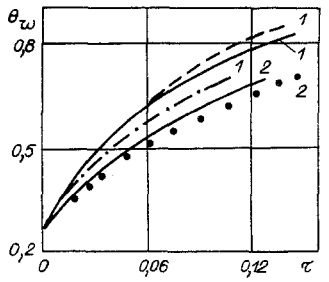

Fig. 5

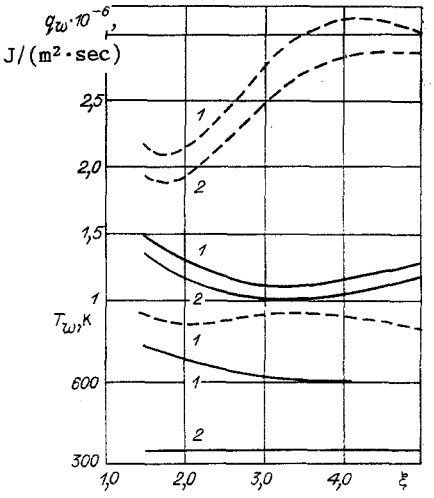

Fig. 6

A comparison of the results of solving the problem in the exact formulation (solid curves), allowing for coupled heat transfer, with the results of solving the problem in the decoupled formulation is shown in Figs. 4 and 5. Here the broken curves denote the solution of the heat-conduction equation with a given heat flux from the gas phase in the form $\tilde{q}_w(\xi) = \frac{q_w(\xi)}{q_w(\xi_*)}\tilde{q}_w(\xi_*)$, where $q_w(\xi)/q_w(\xi_*)$ is taken from Eq. (2.2), and for $\tilde{q}_w(\xi_*)$ we use the well-known formula [15], written for a perfect gas. The dot–dash curves were obtained for the case when we neglect terms with $\partial g_w/\partial\xi$ in Eqs. (2.2)-(2.4), i.e., $\beta = 0$. The curves with the crosses were found for a given heat flux from the gas phase in the form $\tilde{q}_w(\xi) = \frac{St(\xi)}{St_0}\tilde{q}_{w0}$, where the ratio of $St(\xi)/St_0$ was taken from Eq. (2.1).

Figure 4 compares the different approaches for $\tau = 0.108$ and Fig. 5 shows the dynamics of the variation of θ_w as a function of time at various sections along the generators (the curves are 1) $\xi = 1.41$, 2) $\xi = 5.01$).

It follows from a comparison of the curves of $\theta_w(\xi)$ in the region adjacent to the spherical blunting, where the values of the derivatives $\partial\theta_w/\partial\xi$ are substantial, that one should take into account the contribution of the local derivative and should also allow for the prehistory of the development of the thermal boundary layer. For the section of the conical surface where the flow characteristics vary only slightly, with the decoupled method of solving the problem we should neglect the term with $\partial g_w/\partial\xi$ in the formula for the heat-transfer coefficient. In this case we have good agreement with the exact solution when St/St_0 is assigned from Eq. (2.1), which corresponds to assigning the heat-transfer coefficient from the gas phase for the isothermal surface.

We note that for large times τ with the given adiabatic condition on the inner wall of the shell the temperature across the shell is equalized, and for a small value of the parameter π_σ the value of θ_w becomes close to the temperature of the adiabatic surface, which can

be estimated beforehand. We shall consider further the results of calculating the boundary problem of Eqs. (1.1)-(1.7) with typical conditions of motion for dissociated air.

Figure 6 shows the distribution of heat flux q_w and surface temperature T_w on the windward side of the cone $\eta = 0$ at various times (curve 1 is for t = 2 sec, curve 2 is for t = 0). The calculations were performed for $R_N = 0.1$ m, $L/R_N = 0.1$, $T_{wH} = 350$ K. On the inner wall of the shell made of graphite, we imposed the adiabatic condition, and the thermophysical characteristic of the material were taken from [16]. The solid curves correspond to $\chi = 10°$, and the broken curves to $\chi = 20°$.

For the times examined the heat flux values increase as the height decreases because of increased density of air in the incident flow, and here for the motion with $\chi = 20°$ the value of q_w is increased appreciably compared with $\chi = 10°$, which leads in the first case to large value of T_w. The form of the distribution of $T_w(\xi)$ around the body is due to the behavior of the pressure at the outer edge of the boundary layer for the different angles of attack. We correlated the present results, and also results obtained in flight with constant stagnation parameters in the form of the ratio

$$\frac{St}{St_0} = \frac{q_w(\xi, \eta)\,[1 - g_{w0}]}{q_{w0}\,[1 - g_w(\xi, \eta)]}.$$

For the data of Fig. 6 the enthalpy factor is small and varies in the range 0.011 to 0.030. Here the ratios St/St_0 for the constant initial and the variable ambient temperatures are close, and this also follows from analysis of the analytical solution obtained. With a considerable increase of surface temperature the values of St/St_0 at different times can differ appreciably in the region adjacent to ξ_1. Therefore, for such conditions, in solving the problem of heating in the decoupled formation with assigned flux or heat-transfer coefficient from the gas phase, we must take account of the nonisothermal distribution of surface temperature along the generator in this region. For an increase of in the region where the flow characteristics vary only slightly we can use the heat-transfer coefficient found for the isothermal body surface.

LITERATURE CITED

1. A. V. Lykov, Heat and Mass Transfer (Handbook) [in Russian], Énergiya, Moscow (1972).
2. V. I. Zinchenko, and E. G. Trofimchuk, "Solution of nonsimilar problems in laminar boundary layer theory, allowing for coupled heat transfer," Izv. Akad. Nauk SSSR, Mekh. Zhidk. Gaza, No. 4 (19?7).
3. Yu. D. Shevelev, Three-Dimensional Problems in Laminar Boundary Layer Theory [in Russian], Nauka, Moscow (1977).
4. I. N. Murzinov, "The laminar boundary layer on a sphere in hypersonic flow of equilibrium dissociated air," Izv. Akad. Nauk SSSR, Mekh, Zhidk. Gaza, No. 2 (1966).
5. O. N. Suslov, G. A. Tirskii, and V. V. Shchennikov, "Description of flows, in chemical equilibrium, of multicomponent ionized mixtures in the framework of the Navier–Stokes and the Prandtl equations," Zh. Prikl. Mekh. Tekh. Fiz., No. 1 (1971).
6. N. D. Vvedenekaya, "The three-dimensional laminar boundary layer on a blunt body," Izv. Akad. Nauk SSSR, Mekh. Zhidk. Gaza, No. 5 (1966).
7. A. V. Antonets, "Calculation of three-dimensional supersonic flow over blunt bodies with bends in the generators, allowing for equilibrium and frozen states of the gas in the shock layer," Izv. Akad. Nauk SSSR, Mekh. Zhidk. Gaza, No. 2 (1970).
8. Yu. S. Zav'yalov, B. I. Kvasov, and V. L. Miroshnichenko, Spline Function Methods [in Russian], Nauka, Novosibirsk (1980).
9. A. M. Grishin, V. N. Bertsun, and V. I. Zinchenko, The Iteration-Interpolation Method and Its Application [in Russian], Tomsk State Univ. (1981).
10. F. G. Blottner, "Investigation of some finite-difference techniques for solving the boundary layer equations," Computer Methods in Applied Mechanics and Engineering, No. 6 (1975).
11. G. F. Widhopf and R. Hall, "Transitional and turbulent heat transfer measurements on a yawed blunt conical nose-tip," AIAA J., 10, No. 10 (1972).
12. J. W. Cleary, "Effects of angle of attack and nose bluntness on the hypersonic flow over cones," Paper AIAA N 66-414, N.Y. (1966).

13. E. A. Zemlyanskii and G. N. Stepanov, "Calculation of heat transfer in three-dimensional flow of hypersonic air over slender blunted cones," Izv. Akad. Nauk SSSR, Mekh. Zhidk. Gaza, No. 5 (1981).
14. I. R. Brykina, I. A. Gershbein, and S. V. Peigin, "The laminar three-dimensional boundary layer on a permeable surface in the vicinity of the plane of symmetry," Izv. Akad. Nauk SSSR, Mekh. Zhidk. Gaza, No. 5 (1980).

SPECTRAL CHARACTERISTICS OF TWO-DIMENSIONAL TURBULENT CONVECTION IN A VERTICAL SLOT

V. A. Barannikov, P. G. Frik, and V. G. Shaidurov

UDC 532.517.4

The spatial spectra of two-dimensional turbulent convection are obtained in [1]: the velocity fluctuation energy in a developed turbulent convective flow follows the law $E(k) \sim k^{-11/5}$ while the temperature fluctuation energy follows $E_T(k) \sim k^{-7/5}$. The possibility of realizing turbulent flow with such spectral dependences in a vertical slot with heat insulated boundaries is shown there. The energy distribution over the spectrum depends substantially on the heat elimination conditions on the slot side walls. Flow in a slot with ideally heat conductive walls is examined in this paper. The exponential realization of plane turbulent flow in a Hele–Shaw convective cell heated from below which is formed by plates conducting heat well with a linear temperature distribution along the height is described.

1. Incompressible viscous fluid flow is considered in a plane vertical layer of thickness d with the characteristic dimension $\ell \gg d$ (Fig. 1), with boundaries of infinite heat conductivity and the vertical temperature gradient $\partial T/\partial y = -a$. The motion is considered planar ($\mathbf{v} \gg (v_x, v_y, 0)$) with a given velocity profile and temperature across the layer

$$\mathbf{v} = \mathbf{v}(x, y, t) \sin(\pi z/d), \quad T = -ay + \Theta(x, y, t) \sin(\pi z/d). \tag{1.1}$$

Substitution of (1.1) in the equation of thermogravitational convection in the Boussinesq approximation [2] with subsequent integration with respect to z between 0 and d results in two-dimensional equations which take the form after being made dimensionless

$$\partial \mathbf{v}/\partial t = -(\pi/4)(\mathbf{v}\nabla)\mathbf{v} - \nabla p + \Delta \mathbf{v} - D\mathbf{v} + \xi \mathrm{Gr}(\Theta - y); \tag{1.2}$$

$$\partial \Theta/\partial t = -(\pi/4)(\mathbf{v}\nabla)\Theta + (\Delta\Theta - D\Theta)/\mathrm{Pr} + \mathbf{v}\xi; \tag{1.3}$$

$$\nabla \mathbf{v} = 0. \tag{1.4}$$

Here $\mathrm{Pr} = \nu/\chi$ is the Prandtl number; $\mathrm{Gr} = g\beta l^4 a/\nu^2$, Grashoff number; ν, viscosity; χ, thermal diffusivity; β, coefficient of thermal expansion; ξ, a unit vector along the y axis; $D = \pi^2 l^2/d^2$, friction (viscous in (1.2) and thermal in (1.3)) on the side walls of the cavity. Selected as units for measuring the length, time, velocity, and temperature are ℓ, ℓ^2/ν, ν/ℓ, $a\ell$.

The spectral characteristics and investigated on the basis of a hierarchical model of turbulent convection constructed in [1] by projecting the equations of motion (1.2) on a special basis describing the hierarchy of the vortices and thermics of progressively diminishing scale

$$\mathbf{v} = \sum_{N,n} A_{Nn}(t)\, \mathbf{v}_{Nn}(x, y), \quad \Theta = \sum_{N,n} C_{Nn}(t)\, \Theta_{Nn}(x, y).$$

A singularity of the basis functions is the fact that the functions with different subscript N corresponding to the vortex dimension have Fourier transforms that do not overlap in the

Perm. Translated from Zhurnal Prikladnoi Mekhaniki i Tekhnicheskoi Fiziki, No. 2, pp. 42-46, March-April, 1988. Original article submitted December 25, 1986.

 0021-8944/88/2902-0196$12.50